Materials Advances

ROYAL SOCIETY OF CHEMISTRY

REVIEW

View Article Online
View Journal | View Issue

Cite this: *Mater. Adv.*, 2024, 5, 8772

From non-aqueous liquid to solid-state Li–S batteries: design protocols, challenges and solutions

Yuxuan Zhang,[a] Fei Qin,[a] Jinwook Baek,[a] Dong Hun Lee,[a] Minyoung Kim,[a] Han-Wook Song[b] and Sunghwan Lee *[a]

Received 29th June 2024,
Accepted 29th September 2024

DOI: 10.1039/d4ma00666f

rsc.li/materials-advances

Traditional Lithium-ion batteries may not satisfy the requirements of advanced batteries, demanding higher energy and power density, broader operating temperature ranges, and faster charging speeds. Solid-state Li–S batteries (SSLSBs) offer significant advantages, including higher theoretical specific capacity, cost-effectiveness, and environmental benefits. This mini-review exclusively introduces design protocols with emphasis on key governing parameters of SSLSBs towards achieving a specific energy of more than 500 W h kg^{-1}. In addition, the distinct fading mechanisms of SSLSBs compared to non-aqueous electrolyte systems and other ASSB systems are summarized and compared. Then, we outline the state-of-the-art strategies to enhance the electrochemical performance of SSLSBs and suggest insightful directions for future research. This review may be of significance to the design of advanced SSLSBs, by mitigating technical challenges, and hence facilitating their practical implementation in energy storage technologies.

1. Introduction

Traditional non-aqueous liquid electrolyte batteries struggle to meet the stringent requirements, such as higher energy and power density, broader operating temperature ranges, and faster charging speeds, of next-generation electric vehicles (EVs) and electric vertical take-off and landing aircraft (eVTOLs).[1–5] In contrast, solid-state batteries are emerging as a promising alternative, offering significantly enhanced energy density, improved charging and discharging capabilities at higher current densities, and stable operation under extreme temperatures.[6,7] Among these, solid-state Li–S batteries (SSLSBs) are gaining particular interest due to the sulfur cathode's notable advantages, including a high theoretical specific capacity of 1675 mA h g^{-1}, cost-effectiveness, and environmental friendliness.[8,9]

While numerous reviews on SSLSBs have been published, they often neglect material-specific properties and interfacial compatibilities between electrode materials, electrolyte types, and battery components.[10–13] Specifically, systematical comparisons among SSLSBs over traditional Li-ion batteries, $LiNi_xMn_yCo_{1-x-y}O_2$ (NMC) cathode Li metal batteries, and other types of solid-state batteries in terms of key merit parameters have not been comprehensively discussed. Quantitative analysis of key designing parameters (such as sulfur utilization ratio and negative-to-positive electrode material, N/P ratio) for realizing high-energy-density SSLSBs has yet to be presented. In addition, the unique problems of SSLSBs need to be decoupled from the common problems faced by ASSBs to facilitate the development of design and modification strategies specifically for SSLSBs.

This mini-review aims to address these gaps by providing a detailed quantitative comparison between non-aqueous liquid electrolyte Li–S batteries, NMC cathode Li metal batteries, solid-state batteries with NMC cathodes, and solid-state batteries with sulfur cathodes, highlighting the advantages of SSLSBs. We will introduce a design protocol for SSLSBs, focusing on key parameters critical in battery manufacturing. Additionally, we will explore and elaborate on the unique fading mechanisms of SSLSBs, contrasting them with those found in non-aqueous liquid electrolyte systems. Furthermore, we will summarize state-of-the-art modification strategies aimed at enhancing the electrochemical performance of SSLSBs. Finally, this review will provide perspectives on future research and development efforts needed to transition from non-aqueous liquid electrolyte Li–S batteries to SSLSBs, covering various aspects of this evolution.

By filling the knowledge gap concerning the newly emerged SSLSBs, this mini-review may offer guidelines for the battery

[a] *School of Engineering Technology, Purdue University, West Lafayette, IN 47907, USA. E-mail: sunghlee@purdue.edu*
[b] *Convergence Research Center for Meta-Touch, Korea Research Institute of Standards and Science (KRISS), Daejeon 34113, Republic of Korea*

community that seeks the further development of SSLSBs and guide researchers and engineers toward innovations that harness the full potential of this promising technology.

2. Merit comparisons of electrochemical technologies for advanced batteries

In the rapidly evolving landscape of energy storage technology, the demand for next-generation EVs, eVTOLs, and high-altitude pseudo-satellites (HAPS) is driving the need for superior battery solutions. Current lithium-ion batteries (LIBs) fall short of meeting the stringent requirements for these cutting-edge applications as indicated in Fig. 1(a).[1,14,15] LIBs typically offer energy densities of 150–250 W h kg^{-1}, while future EVs, eVTOLs, and HAPS demand upwards of 300–500 W h kg^{-1}.[16–18] Additionally, current LIBs face challenges in achieving fast charging times, with significant safety concerns such as thermal runaway and fire risks due to flammable non-aqueous electrolytes.[18–20] The electrochemical performance of LIBs also degrades in low temperatures because the ion mobility of non-aqueous electrolytes will be largely affected by the low temperature.[21–23] In contrast, all solid-state batteries (ASSBs)

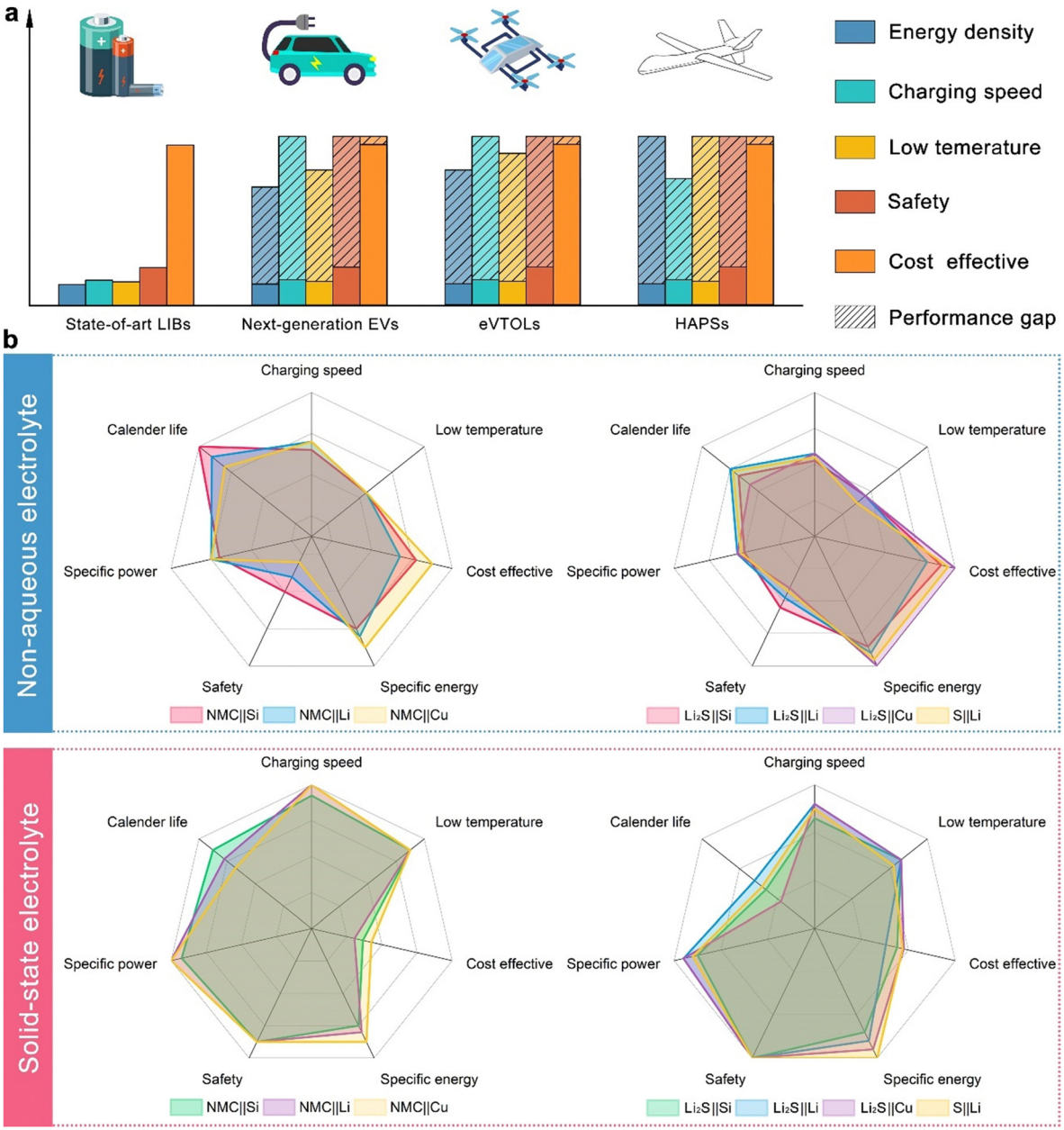

Fig. 1 (a) Comparison of the requirements of next-generation EVs, eVTOLs, and HAPSs with state-of-the-art LIBs in terms of energy density, charging speed, low-temperature performance, safety, and cost-effectiveness. (b) Radar plots of batteries with different configurations in both non-aqueous electrolytes and SSEs.

promise energy densities exceeding 500 W h kg^{-1}, faster charging times due to better ion transport through solid electrolytes, superior low-temperature performance, and enhanced safety by eliminating flammable components.[24–27] Although currently more expensive, advancements in ASSB technology are expected to reduce costs, making them a more viable option in the long term.[28–30]

Despite having the highest theoretical capacity, solid-state Li–air batteries are viewed as a long-term prospect due to numerous and severe technical challenges that are unlikely to be resolved at this stage.[31] On the other hand, due to the successful commercialization of NMC cathodes, ASSBs with NMC cathodes have garnered significant attention in both academia and industry. As a result, ASSBs with NMC cathodes are selected as the primary competitors to SSLSBs in this comparison. The comparative analysis of various battery configurations, as illustrated by radar plots, provides a detailed examination of the performance metrics of NCM||Si, NCM||Li, NCM||Cu (Cu denotes anode-free), Li_2S||Si, Li_2S||Li, Li_2S||Cu, and S||Li in both non-aqueous electrolyte systems and solid-state systems. The non-aqueous configurations reveal that the safety issue is still challenging for the application of Li metal batteries and anode-free batteries.[32–34] However, contributed by the inflammable SSEs, the safety of ASSBs has been largely increased.[35–37] The increased safety of ASSBs allows the application of thermal-promoted fast charging without concern about thermal runaway.[38,39] In addition, the ion mobility of SSEs will not be decreased in low-temperature conditions as in non-aqueous electrolyte systems, leading to excellent low-temperature electrochemical performance.[40–42] The enhanced safety, ability to operate under extreme conditions, and higher energy density compared to non-aqueous liquid Li–S batteries make SSLSBs a more suitable choice for space missions.[43] However, the relatively short cycle life and high manufacturing cost of ASSBs are some of the major issues that need to be resolved before commercialization, the detailed causation of which will be discussed in the following section.[44–46]

Having established the comparative performance metrics of various battery configurations in both non-aqueous and solid-state systems, it becomes evident that the choice of cathode material plays a crucial role in optimizing battery performance for next-generation applications.[47–49] The element abundance, price, and toxicity need to be considered due to their significant impact on the commercialization of battery materials.[50,51] We compared the earth's abundance, price, and toxicity of elements in NMC cathodes and sulfur-based cathodes (Fig. 2). The use of Cobalt in cathode materials poses several significant resource-related challenges that affect its feasibility and sustainability.[52–54]

Cobalt is relatively scarce, with an estimated earth abundance of 185 000 tons, compared to 56 300 000 tons of sulfur, 2 200 000 tons of nickel, and 9 800 000 tons of manganese.[55–57] This scarcity makes cobalt a critical material, subject to supply constraints and potential shortages as battery demand increases. The battery industry, which uses large amounts of cobalt in cathode materials like lithium cobalt oxide, NMC, and

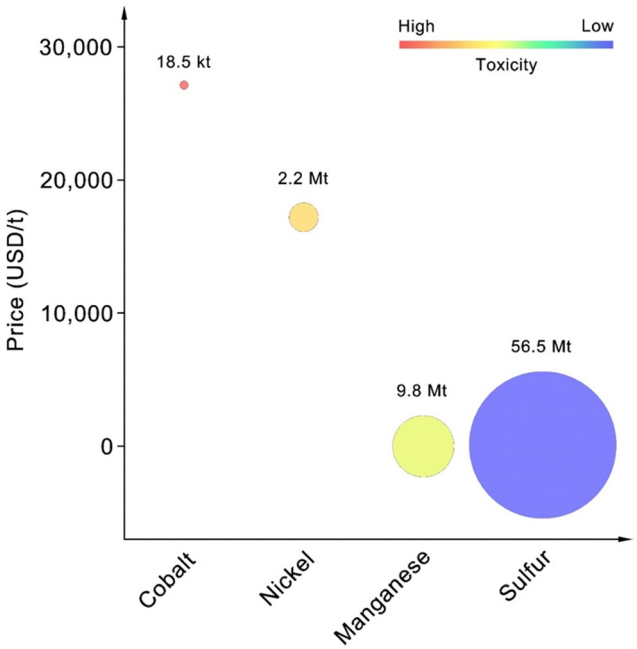

Fig. 2 Earth abundance, price, and toxicity of different elements (earth abundance was indicated by the size of circles).

$LiNi_xCo_yAl_{1-x-y}O_2$ (NCA), accounts for about 50% of the total demand for cobalt.[58,59]

While cobalt enhances specific energy and structural stability in cathode materials, it also presents challenges such as toxicity, high cost (around $27 000 per ton), limited production, and restricted reserves.[58] Additionally, the geographic concentration of cobalt deposits creates supply chain risks. Although cobalt-free cathodes are a promising alternative, they face challenges in matching the performance metrics of cobalt-containing cathodes, potentially resulting in lower energy densities and reduced cycle life.[60,61]

However, nickel is irreplaceable as a core component of NMC and NCA cathodes, providing charge compensation during the charge and discharge processes.[62,63] Despite its essential role, nickel's price is second only to cobalt, at approximately $17 000 per ton, significantly higher than sulfur's $100 per ton.[64] Additionally, nickel is more toxic than sulfur, as shown in Fig. 2.

Therefore, from the perspective of long-term development goals, using sulfur as the element for developing the next generation of high-energy-density cathodes is very promising.

3. Designing protocols for high-energy-density SSLSBs

Sulfur is inexpensive, widely available, and has low toxicity, making it an attractive option for future battery technologies, which becomes imperative to explore and optimize sulfur-based cathodes for next-generation battery technologies. The inherent properties of sulfur not only make it a more sustainable choice but also offer the potential for higher energy

densities, which are crucial for advancing energy storage systems. However, the practical implementation of SSLSBs is limited due in part to a lack of comprehensive analyses of key performance parameters affecting the energy density of SSLSBs. A detailed understanding is required of how governing factors, such as mass loading, sulfur content, sulfur utilization ratios, the mass ratio of the electrolyte-to-sulfur (E/S) ratios, and the capacity ratio of the N/P ratios, influence the overall performance of these batteries. To investigate the effect of various key parameters on the specific energy of SSLSBs, the intricate relationship between these variables and their impact on the energy density of SSLSBs have been quantitively bridged through a theoretical calculation.[65]

SSLSBs are composed of several key components: active materials, inactive materials, current collectors for electron transport, SSEs layer for ion transport, and a package to shield the battery core from air. Herein, we will exclude the package weight to simplify the calculation process.

The specific energy of the pouch cell was calculated based on the equation:[66]

$$W = E_{\text{Theoretical}} \times R_{\text{SUR}} \times R_{\text{M}}$$

where, $E_{\text{Theoretical}}$, R_{SUR}, and R_{M} represent the theoretical specific energy of the selected system, sulfur utilization ratio, and mass ratio respectively. The sulfur utilization ratios of 60%, 70%, 80%, 90%, and 100% are selected in this calculation. R_{M} is defined as the following equation:

$$R_{\text{Weight}} = \frac{\frac{M_{\text{Li}_2\text{S}}}{M_{\text{s}}} \times m_{\text{sl}}}{\frac{m_{\text{sl}}}{R_{\text{Cathode}}} + \frac{m_{\text{Al}} + m_{\text{Cu}}}{2} + R_{\text{E/S}} \times m_{\text{sl}} + \frac{2M_{\text{Li}}}{M_{\text{s}}} \times R_{\text{N/P}} \times m_{\text{sl}}}$$

here, $M_{\text{Li}_2\text{S}}$, M_{S}, and M_{Li} represent the molar weights of Li_2S (45.947 g mol^{-1}), sulfur (32.065 g mol^{-1}), and lithium (6.941 g mol^{-1}), respectively. The symbol m_{sl} denotes the areal mass loading of sulfur in the cathode. R_{Cathode} represents the weight ratio of sulfur in the cathode, which includes the sulfur, host, conducting agent, and binder. m_{Al} and m_{Cu} are the areal masses of the aluminum current collector and copper current collector, respectively. $R_{\text{E/S}}$ is the ratio of electrolyte to sulfur (in mg to mg), and $R_{\text{N/P}}$ is the ratio of the theoretical areal capacity of the lithium metal negative electrode to that of the sulfur positive electrode. To simplify the calculations, we use the following parameters commonly applied in real pouch cells: the thickness of the aluminum foil is 10 μm with an areal density of 2.7 mg cm^{-2}, and the copper current collector is 10 μm thick with an areal density of 8.9 mg cm^{-2}.

By optimizing R_{SUR}, and R_{M}, Li–S batteries can achieve high energy densities. For instance, a Li–S battery with $R_{\text{M}} \geq 28\%$ and $R_{\text{SUR}} \geq 70\%$ can achieve an energy density of 500 W h kg^{-1}. Future advancements should focus on reducing electrolyte-to-sulfur ratios, enhancing sulfur loading, and improving the stability of lithium anodes to achieve even higher energy densities and practical applications in energy storage systems.

Based on the derived formula above, the energy density is related to five parameters: mass loading, sulfur content, sulfur utilization ratios, E/S ratios, and N/P ratios. We configured surface plots in Fig. 3 showing the relationship between energy density and each of the parameters while fixing the other parameters.

The 3D curve diagram in Fig. 3(i)–(iii) indicates that, a sulfur loading of at least greater than 4 mg cm^{-2} is a prerequisite in the S||Li SSLSB to secure the energy density greater than or equal to 500 W h kg^{-1}. However, subsequent increases in sulfur loading have a very limited effect on overall energy density improvement. Reducing the N/P ratio significantly contributes to the overall energy density enhancement, especially when the N/P value approaches 1. Therefore, it is essential to minimize the N/P value while ensuring the electrochemical reversibility of the battery. Of note, the diagram also shows that improving the sulfur utilization ratio has a more significant effect on increasing energy density compared to increasing sulfur content or decreasing E/S. Therefore, after achieving a sulfur loading of 4 mg cm^{-2}, priority should be given to improving the sulfur utilization ratio to maximize the benefits of increasing the overall energy density of the battery. In contrast, the benefits of increasing sulfur content are minimal. Even though the sulfur content nearly doubles (from 50% to 90%), this change has a very limited effect on the overall energy density. The same situation is observed in the anode-free system Li_2S||Cu, where the improvement in energy density from changing sulfur content is almost negligible. However, increasing the sulfur utilization ratio still remarkably enhances the overall energy density. It is worth noting that in the anode-free system, the impact E/S ratio on the increase of the overall energy density becomes very powerful. When E/S is less than 5, further reducing E/S results in increased benefits for energy density. The volume of the stacking battery based on the anode-free Li_2S||Cu system is lower than that of the S||Li system when the thickness of other components in the battery is kept constant as illustrated in Fig. 3. This reduction in volume potentially leads to a higher volumetric energy density for the anode-free system.

Therefore, based on the analysis of multiple 3D curve plots, our conclusions on designing high-energy-density SSLSBs are as follows:

1. For SSLSB with lithium metal anode, after achieving a sulfur loading of 4 mg cm^{-2}, priority should be given to improving the sulfur utilization ratio. For example, introducing a catalyst may reduce sulfur content, but since the sulfur utilization ratio is improved, the overall energy density will still be enhanced.

2. Reducing the N/P ratio is crucial for overall energy density enhancement, provided the anode's reversibility is ensured. Therefore, optimizing the reversibility of the anode (Li deposition and stripping) becomes essential.

3. For anode-free SSLSBs, both improving sulfur utilization ratio and E/S are effective methods to increase energy density. When E/S is below 5, further reducing E/S significantly enhances the benefits. Hence, developing stable ultrathin solid electrolyte layers is crucial for improving energy density.

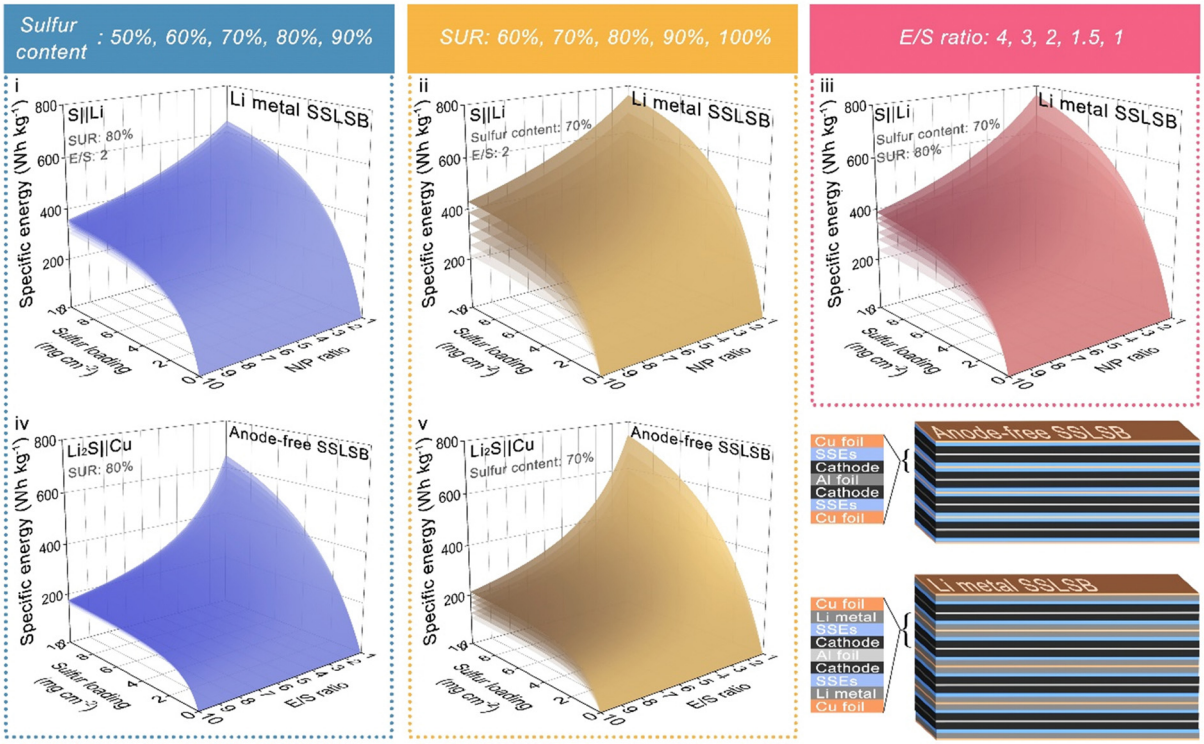

Fig. 3 The energy density of SSLSB (S||Li top, Li_2S||Cu bottom) in terms of various sulfur loading, sulfur content, sulfur utilization ratio, E/S ratio, and N/P ratio and the schematic of stacked SSLSBs based on S||Li and Li_2S||Cu.

4. General challenges in all-solid-state batteries

All-solid-state batteries (ASSBs) face numerous technical challenges, including interfacial stability, ionic conductivity, and material compatibility.[67] These issues are also present in solid-state lithium–sulfur batteries (SSLSBs).[68,69] Addressing these common problems is crucial for advancing SSLSB development. This section discusses the general problems faced by ASSBs and then delves into the specific challenges unique to SSLSBs, providing valuable insights for research in this emerging field.

4.1 Interfacial instability, dendrite formation, and volume variation

Despite decades of development, solid-state electrolytes (SSEs) have only recently achieved ionic conductivities comparable to conventional aprotic electrolytes. However, ASSBs still struggle with chemical and electrochemical instabilities at electrode–electrolyte interfaces, lithium dendrite formation, and anode volume variation, which significantly impede the energy density, cycle life, and safety of ASSBs. SSLSBs are no exception to these challenges.[68,70]

However, the cathode–electrolyte interface in SSLSBs is more stable than that in NMC-based ASSBs. The interface instability in SSLSBs primarily arises from the anode–electrolyte interface, leading to a low reversible lithium-ion stripping-plating process and the parasite reactions of the electrolyte adjacent to the anode side as illustrated in Fig. 4(a).[71]

As identified in Fig. 3, energy density in SSLSBs increases significantly with anode-less (N/P = 1 to 1.2) and anode-free (N/P = 0) systems. Nevertheless, the low reversibility and non-uniformity of the lithium-ion stripping-plating process prevent the effective utilization of low N/P ratio systems. Nonuniform lithium deposition can create localized high-current regions, leading to uneven lithium distribution and dendrite formation.[75–77] Additionally, lithium metal may react with the solid electrolyte, leading to its decomposition. For example, sulfide-based electrolytes react with lithium to form lithium sulfide (Li_2S), which impedes ion transport.[78,79]

The volume variation of the lithium metal anode during cycling, due to repeated plating and stripping of lithium, induces mechanical stress on the solid electrolyte and electrode interface.[80,81] This stress can lead to mechanical degradation due to the mismatch in mechanical properties between the lithium metal and the solid electrolyte.[82,83] Furthermore, many solid electrolytes are brittle and prone to cracking under mechanical stress as described in Fig. 4(b). The SEM images showed that the SSE layer was well in contact with the Li metal anode before cycling, whereas void space and vertical cracking were observed after cycling due to the volume variation during the charge and discharge process.[72]

4.2 High manufacturing costs

The high manufacturing costs of ASSBs pose a significant challenge to their application. SSEs are a major contributor to these costs. Sulfide-based SSEs, such as $Li_{10}GeP_2S_{12}$ (LGPS) and Li_6PS_5Cl (LPSC), are known for their high ionic conductivity but

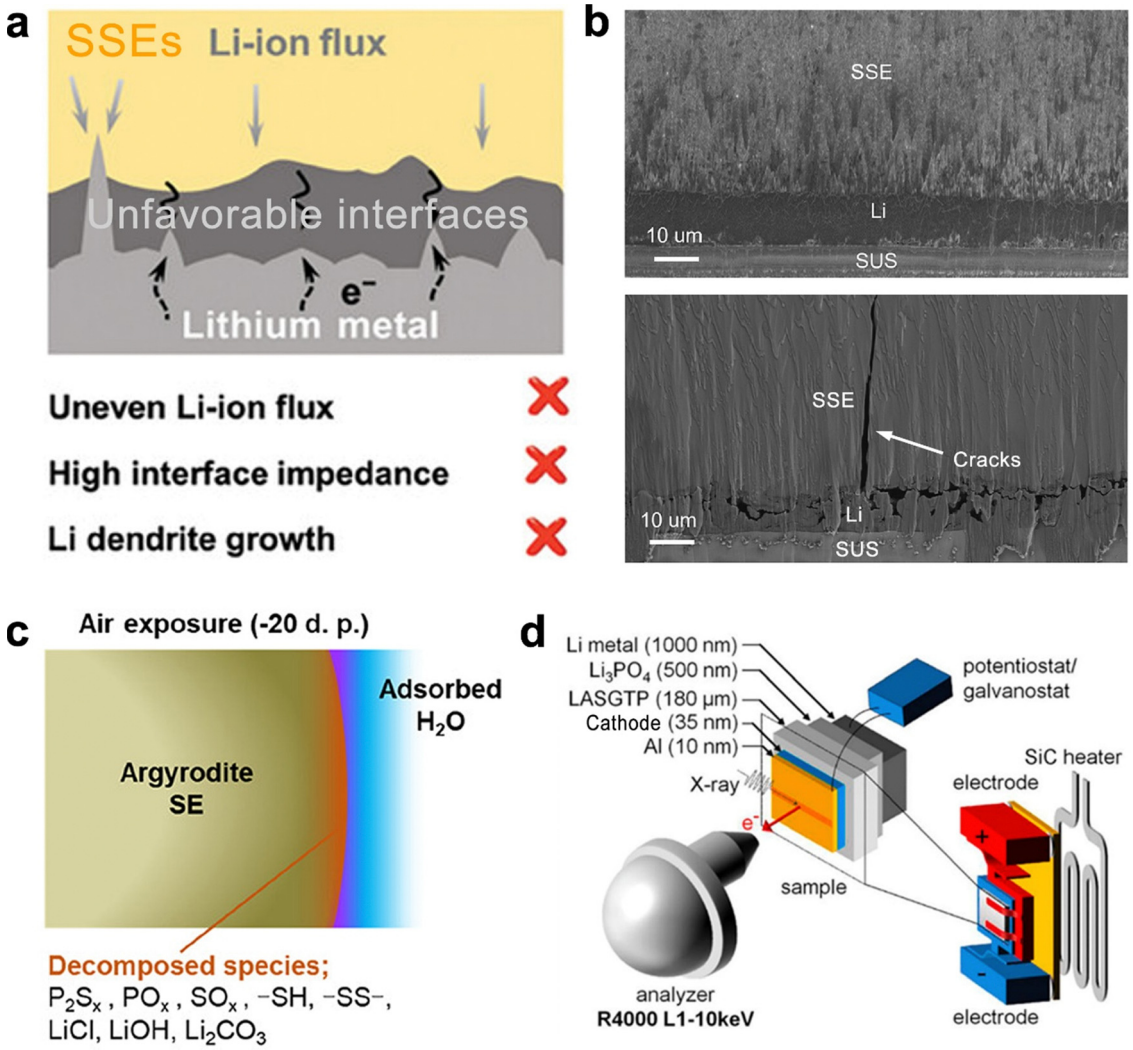

Fig. 4 (a) Schematic of parasite reactions between SSEs and Li metal and the dendrite.[71] (b) Cross-section SEM image of interfacial evolution at SSE/Li before and after 20 cycles.[72] (c) Schematic of the decomposition of LGPS.[73] (d) Schematic of the ASSB and electrochemical setup for operando hard X-ray photoelectron spectroscopy (HAXPES).[74]

are expensive due to costly raw materials and complex synthesis processes.[84] Additionally, these SSEs require challenging storage and manufacturing conditions due to their sensitivity to air and high temperatures.[85]

Sulfide-based SSEs can react with moisture in the air to produce harmful H_2S gas and decompose (Fig. 4(c)), necessitating preparation and handling in an inert gas-filled glovebox.[73] The thermal stability of these electrolytes is also a concern; for instance, Li_7PS_{11} decomposes at temperatures above 280 °C, and LGPS begins to decompose into $Li_4P_2S_6$ at around 600 °C.[86–88] Garnet-type SSEs, like $Li_7La_3Zr_2O_{12}$ (LLZO), are also highly sensitive to ambient air.[89,90] Exposure to air leads to the formation of Li_2CO_3 on the surface due to lithium-ion exchange with protons in moisture, forming lithium hydroxide, which then reacts with CO_2 in the air to form lithium carbonate. Thus, LLZO storage must avoid ambient air to prevent degradation.[91,92]

Thus far, the production of ASSBs is not as mature or scalable as conventional lithium-ion batteries. The lack of established large-scale production lines means that economies of scale cannot be realized, leading to higher per-unit costs. Moreover, the specialized nature of solid-state battery components requires customized manufacturing processes, further driving up costs. Schnell *et al.* highlighted a significant challenge in scaling up the fabrication of ASSBs using oxide SSEs.[93] Mature slurry-based technologies can produce dense layers with high throughput on a large scale, but the required high sintering temperatures prevent the co-firing of SSE and cathode particles. As a result, they proposed that vapor or aerosol deposition methods might be the only viable option to create dense SSE layers without high-temperature sintering for cathode-supported ASSBs, thereby limiting throughput to the layer growth rate.[93]

4.3 Limitations of investigation techniques

Characterizing and investigating charge transfer processes, failure mechanisms, and models in ASSBs is challenging due to the complex and heterogeneous nature of solid-state systems. Multiple interfaces between the solid electrolyte, lithium

anode, and cathode complicate the analysis, particularly for the sulfur conversion process in SSLSBs.

Although *in situ* and operando techniques have advanced significantly, they still face limitations in providing comprehensive information about solid-state systems. Integrating the external pressure applied to ASSBs into these techniques is a major challenge.[94] The size limitations required for samples present another critical barrier to understanding the reaction mechanism in ASSBs. Fig. 4(d) shows an example of a cell design for *in situ* HAXPES, equipped with a SiC heater to analyze the electrochemical process at temperatures higher than room temperature (RT) to improve ionic conductivity.[74] The design is orthogonally aligned with the incident X-ray radiation. However, due to the penetration depth of the X-ray radiation, each component must be as thin as possible. The cathode thickness is only 35 nm, significantly lower than the 40–80 μm thickness of an actual cathode used in ASSBs. This overly thin cathode may not adequately reflect the kinetic conditions originating from porous electrode structures.

Simulations are a powerful tool for investigating ASSBs but bridging different length scales—from atomic-scale interactions to macroscopic battery behavior—remains computationally demanding. Most first-principles research on battery materials has focused on crystalline solids. Simulations of polycrystalline and amorphous structures, as well as grain boundaries, remain underexplored, despite their common occurrence in real battery materials.[68] A fundamental understanding of ion transport through the liquid–solid and polymer–inorganic interface at the atomic level is also lacking.[95] The atomic structure, stoichiometry, chemistry, defects, and microstructures calculated from bulk and interface are not exactly the same. Calculations based on bulk thermodynamics may not fully reflect the actual interface situation.[95,96] Moreover, ASSBs are complex multiphase systems involving electro-chemo-mechanical-thermal behavior or multiphysics. Currently, there is no adequate method or theory for multiscale and multiphysics field research due to the limitations of various calculations.[97]

In recent years, the development of artificial intelligence (AI) has opened new avenues for ASSBs.[67] Traditional "trial-and-error" processes require a vast number of tedious experiments. AI combined with computational chemistry can significantly accelerate the research and development of novel battery systems.[98] However, the inverse design of battery materials, which starts with desired properties as inputs and aims to determine the corresponding structure and composition as outputs, has been computationally infeasible due to its massive complexity.[98] In addition, data scarcity, data interpretability, complexity of battery systems and cost safety are still remaining challenges for AI methodologies applied in the investigation of ASSBs.[99]

5. Specific issues in solid-state lithium–sulfur batteries

The unfavorable kinetic conditions for sulfur conversion significantly hinder SSLSB performance in multiple ways, as illustrated in Fig. 3.

The reaction mechanisms and intermediate chemistries have been extensively studied in liquid Li–S batteries. During galvanostatic discharge, two distinct plateaus correspond to the formation of soluble long-chain (Li_2S_n, $4 \leq n \leq 8$) and solid short-chain (Li_2S_2) polysulfide intermediates.[100] The rate-determining step in non-aqueous Li–S batteries involves the conversion between solid and liquid polysulfides, as well as the solid-to-solid reaction.[101] Understanding this sulfur conversion process facilitates the design of improved Li–S batteries.

A widely accepted explanation for this is the absence of solvation in solid electrolytes (SEs), which prevents the formation of long-chain polysulfides.[102] Another explanation posits that the single plateau generally indicates a direct reaction between S_8 and Li_2S.[103,104] A recent study by Cao *et al.* has further developed the latter explanation by constructing an operando SSLSB system as illustrated in Fig. 5(a).[105] The cell has a side opening for direct laser exposure, avoiding signal loss. A stainless-steel framework controls the pressure, ensuring accurate electrochemical reactions for reliable operando measurements. The square opening helps focus the laser on a flat sample surface, preventing signal issues. The battery components (cathode, SE, and anode) are stacked in a polyether ether ketone (PEEK) die, and the stainless-steel framework maintains high stacking pressure during the test. They suggested that the electrochemical redox reactions involve the conversion of S_8 to Li_2S, with Li_2S_2 as an intermediate phase, while Li_2S_8, Li_2S_6, and Li_2S_4 are not present as indicated in Fig. 5(b). During the discharging process, S_8 first converts to Li_2S_2, which then further reduces to the final product, Li_2S. These reactions reverse during the charging process.

Although the sulfur conversion process in SSLSBs is not yet fully understood, several factors have been identified as major contributors to the unfavorable kinetic conditions.[11,107] Several studies have confirmed that the low electronic conductivity of elemental sulfur and polysulfides is a significant drawback of the sulfur cathode in SSLSBs, which also represents one of the major bottlenecks in non-aqueous electrolyte Li–S systems.[108] The sulfur conversion process, which involves multiple electron transfer steps, has been hindered by the insulating nature of sulfur and its discharge products (Li_2S and Li_2S_2).

The limited conductivity results in poor utilization of the active sulfur material, as only the regions in close contact with conductive additives participate effectively in the electrochemical reactions. Lee *et al.* revealed that electronic conductivity is more critical for the rate and cycle performance of thick electrodes than ionic conductivity, which underscores the need to further optimize electronic conduction in high sulfur loading cathode to enhance the overall battery performance.[109]

The retarded ion transport has often been cited as one of the bottlenecks for the kinetic condition as well. In contrast to the ion transport at the interface between the cathode and the electrolyte, which is the primary kinetic limitation in intercalation-type solid-state batteries, the sluggish ion transport within the bulk of elemental sulfur and polysulfides is a major issue limiting the kinetic conditions in SSLSBs.[110] Bradbury *et al.* revealed that the sluggish effective lithium-ion

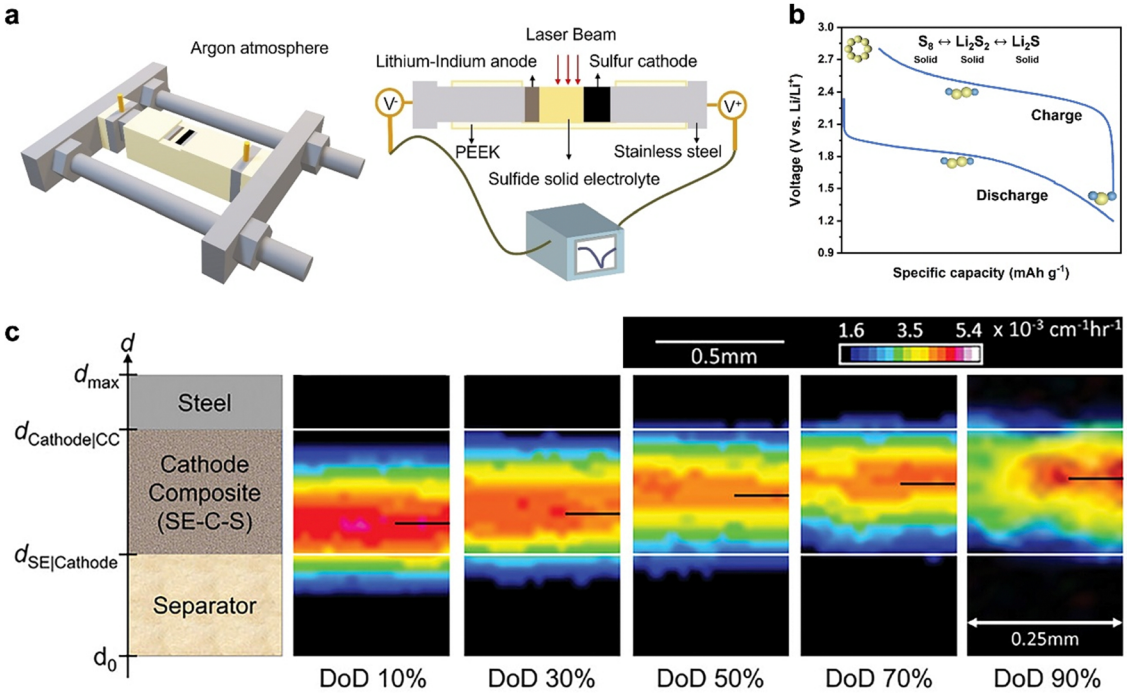

Fig. 5 (a) Schematic of the PEEK cell and the setup for in-operando Raman characterization.[105] (b) A typical charge–discharge profile of SSLSBs. Inset: Schematic of the reaction mechanism.[105] (c) Dynamic evolution of lithium distribution in the SSLSB as the degree of discharge (DoD) increases.[106]

transport in sulfur composites is the rate-limiting factor and leads to a nonuniform reaction (*i.e.*, polarization) *via* 2D radiograph visualization as indicated in Fig. 5(c).[106] The high-intensity region of the 2D radiographs, which represents the position of the ongoing sulfur conversion reaction, creeps from the separator-layer side to the current collector upon the initial discharge. This result extends the porous electrode theory for SSLSBs, confirming that sluggish effective lithium-ion transport in composites is rate-limiting and leads to a nonuniform reaction front.

The volume variation has also been identified as a vital factor for kinetic conditions, especially in the SSLSB system. The sulfur particles may lose contact with the solid electrolyte and the conductive agent due to the 78% volume change in the conversion reaction.[111] Furthermore, the excess volume change may trigger the crack formation in the solid electrolytes and due to the accumulated mechanical stress, disrupt ionic pathways and lead the battery failure.

The notorious "shuttle effect" needs also be considered in polymer electrolyte-based SSLSB systems due to the high solubility of polysulfides in the polymer matrices.[112] However, inorganic solid electrolytes have been confirmed to effectively limit the dissolution of polysulfides due to their low solubility in these electrolytes, thereby mitigating the "shuttle effect".[113]

Even though significant progress has been made in understanding the sulfur conversion process in SSLSBs, the rate-determining step has yet to be identified, which is crucial for developing methodologies to increase the sulfur utilization ratio and accelerate the sulfur conversion process in SSLSBs. Therefore, it is urgently necessary to establish a detailed, convincing, and widely accepted reaction model. To enhance the understanding of the reaction mechanisms in the Li–S system, it is crucial to consider the potential differences in the reaction pathways and rate-determining steps of sulfur conversion. These differences may arise when comparing inorganic solid electrolytes with polymer-based solid electrolytes, as well as when comparing Li_2S cathodes with elemental S cathodes. Therefore, it is essential to take into account these varying conditions to accurately elucidate the reaction mechanisms involved.

6. State-of-art mitigation strategies

The development of SSLSBs is a promising avenue for advancing energy storage technologies due to their high energy density and intrinsic safety benefits. However, several challenges impede their practical application. This section explores various modification strategies aimed at overcoming these issues to enhance the performance and stability of SSLSBs. Mitigation strategies for SSEs engineering and anode protection have been well summarized in many other reviews, which can be referred to for detailed insights.[69,104,114] Most of these modification strategies are universally applicable to all ASSBs, as they address general issues common to SSEs and anodes across these systems. Consequently, our focus here is on mitigation strategies that address the unique challenges specific to SSLSBs, which predominantly arise from the cathode. In SSLSBs, the majority of cathode materials used are pure sulfur and Li_2S. Li_2S is considered a pre-lithiated cathode material,

making it suitable for assembling Li–S batteries with lithium-free anodes. In addition, the volume change effect is minimized when using Li_2S as the cathode material since Li_2S is already the least dense phase with lithium incorporated, which does not expand during battery operation.[115,116] However, Li_2S has a theoretical capacity of only 1166 mA h g^{-1}, which is 70% of that in the sulfur cathode.[117,118] Moreover, Li_2S is more challenging to handle and process due to its hygroscopic nature and sensitivity to moisture.[119] To optimize the performance and practicality of sulfur and Li_2S in SSLSBs, advances in materials design and processing techniques continue to address challenges of both types of cathodes of are involved in the following section.

6.1 Engineering electronic/ionic conductivity

The sulfur utilization ratio is directly related to the low electronic and ionic conductivities of polysulfides. Developing nano-sized sulfur–carbon composites where sulfur is uniformly dispersed within a conductive carbon matrix is an effective way to enhance electronic conductivity and sulfur utilization. However, the traditional selection principle of carbon materials in the liquid lithium–sulfur batteries may not be fully applicable in SSLSBs due to the lack of infiltrating liquid electrolytes, which results in difficult ion transport within the composite cathode.

Multiple manufacturing strategies including solution reaction infusion, mechanical milling, and vapor deposition have been demonstrated to integrate carbonaceous matters with sulfur-based cathode materials. For example, reduced graphene oxide (rGO) can be coated on amorphous sulfur nanolayers to maintain high electronic conduction and shorten the ionic pathway *via* a solution process.[120] Additionally, a ball milling method followed by heat treatment has been reported to synthesize a Li_2S@C nanocomposite with Li_2S nanocrystals uniformly embedded in the conductive carbon matrix.[121] The *in situ* generated carbon is intimately wrapped on the nano-sized Li_2S particles, which greatly enhances the electronic conductivity, and effectively prohibits the aggregation of Li_2S nanoparticles. In addition, a nanoscale percolation network can be formed to offer effective pathways for both electrons and ions and alleviate the stress/strain during lithiation/delithiation. However, it is believed that conventional approaches in the synthesis of sulfur–carbon composites *via* mechanical milling and solution process make it hard to achieve a homogenous distribution of sulfur within a carbon matrix, which is critical to making high-performance SSLSBs. A sulfur vapor deposition approach (Fig. 6(a)) has been demonstrated as an effective way to realize a homogenous distribution of sulfur in the carbon matrix.[122] High-angle annular dark-field (HAADF) TEM imaging of the sulfur–carbon composite (Fig. 6(b)), along with the corresponding electron energy loss spectroscopy (EELS) elemental mapping (Fig. 6(c)), reveals overlapped sulfur and carbon traces, indicating a homogeneous sulfur distribution within the porous carbon at the nanoscale. In addition to introducing carbon additives, other conductive polymers such as polyaniline,[123] poly(3,4-ethylenedioxythiophene),[100] polypyrrole,[124] and polythiophene[125] have also been employed to improve the conductivity of the sulfur cathode materials. However, inducing conductive agents (*i.e.*, carbonaceous materials and conductive polymers) will inevitably reduce the active material (sulfur) content in the cathode. More importantly, the introduced conductive agents may lead to the degradation of SSEs at the interface of conductive agents and SSEs due to the limited compatibility of the dissimilar materials contact. Therefore, tuning the intrinsic conductivity of sulfur cathode materials by introducing other elements into sulfur cathode has populated in recent years.[122] For example, the electronic conductivity of the SeS_x solid solution has been improved to 1×10^{-3} S cm^{-1} compared to the 0.5×10^{-27} S cm^{-1} of pure S.[126,127] Then the SeS_x solid solution was mixed with Li_3PS_4, which is a high ionic conductor, to form the cathode of SSLSBs.

Doping multivalent cations can enhance the ionic conductivity of Li_2S. Atsunori *et al.* prepared $Li_{2-3x}Al_xS$ by doping Li_2S with Al_2S_3.[131] The addition of Al^{3+} creates defects in the Li_2S structure, improving its electronic/ionic conductivity and lowering the activation energy barrier. The cell with x = 0.1667 showed an increase in capacity from 600 mA h g^{-1} to over 800 mA h g^{-1} in the first 10 cycles, maintaining around 800 mA h g^{-1} after 50 cycles. In a most recent study, Iodine was adopted to fabricate $S_{9.3}I$ through a grinding and heating process.[128] The synthesized $S_{9.3}I$ delivered electrical conductivity of 5.9×10^{-7} S cm^{-1} at room temperature, which is approximately semiconductor level. DFT calculations revealed that the introduction of Iodine adds states within the band gap and reduces the band to 1.65 eV, compared to 2.92 eV of the non-doped counterpart, as indicated in Fig. 6(d). $S_{9.3}I$ exhibits a lower melting point at around 65 °C, which allows the integration of a thermal system to melt the discharge products for achieving a healable interface as indicated in Fig. 6(e).

6.2 Metal sulfide additives

Incorporating catalytic additives such as transition metal sulfides or oxides can accelerate the conversion of polysulfides to Li_2S, thereby increasing the sulfur utilization ratio. Metal sulfides, including VS_2, CuS, FeS_2, and Al_2S_3 have been identified as beneficial components in sulfide-based Li–S batteries due to their compatibility with both sulfur and sulfide electrolytes for a long time.[132–134] In 2004, Hayashi and colleagues discovered that the performance of SSLSBs varies significantly with the molar ratio of the S/Cu composite cathodes, where the sulfur and copper were mixed in different ratios and subjected to varying milling times.[135] The battery utilizing a cathode material with a S/Cu ratio of 3, prepared by milling for 15 minutes, demonstrated the best electrochemical performance, achieving a discharge capacity of over 650 mA h g^{-1} for 20 cycles.

Many metal sulfide materials that perform poorly in liquid batteries tend to exhibit superior electrochemical performance in solid-state batteries due to the elimination of the ''shuttle effect'', which is also *vice versa*.[136] Kim *et al.* compared the electrochemical behavior of SnS materials in both solid-state and liquid batteries.[129] The SnS-based solid-state batteries

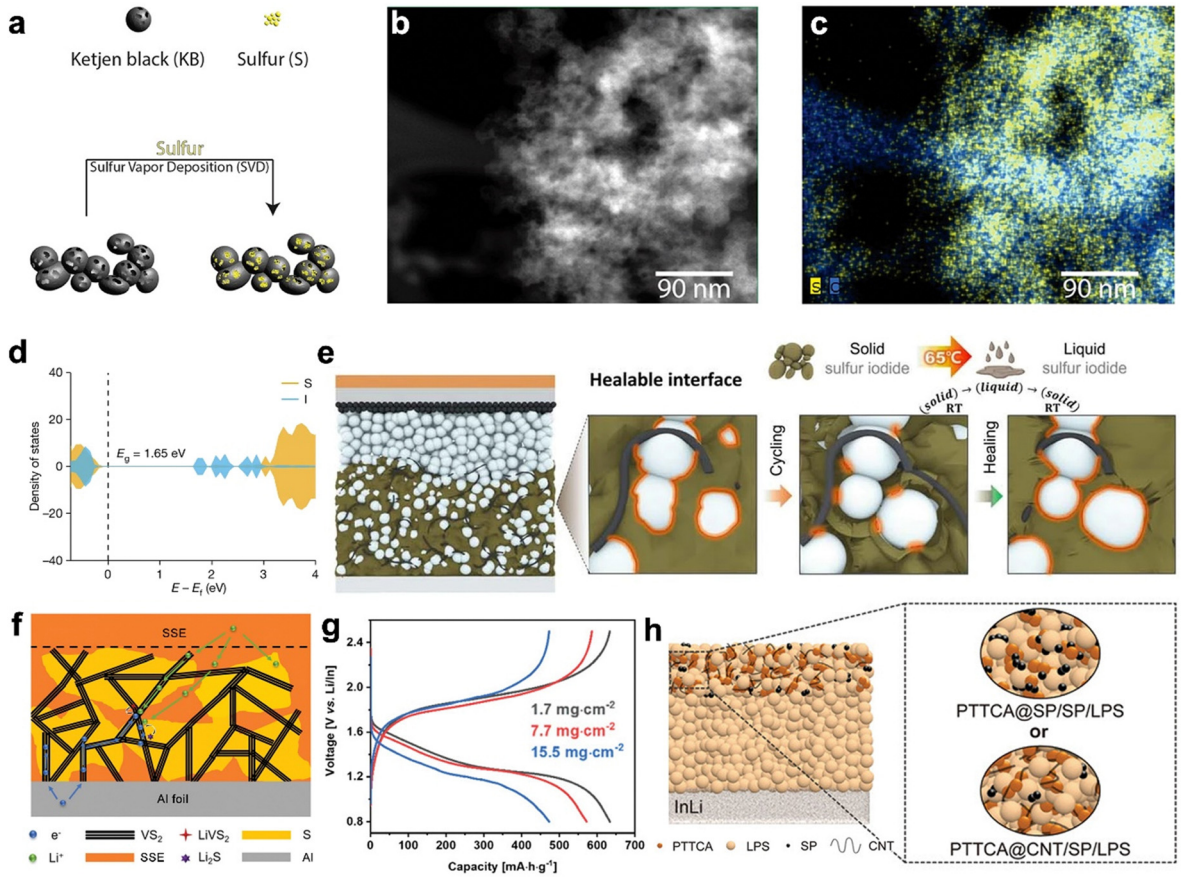

Fig. 6 (a) Schematic illustration of the synthesis of the cathode using the vapor deposition method.[122] (b) HAADF image and (c) EELS elemental mapping of sulfur cathode synthesized *via* vapor deposition method.[122] (d) Elemental projected density of states for $S_{9.6}I$ from DFT calculations.[128] (e) Schematic of the SSLSB with S9.6I as the active material, achieving ideal active material/electrolyte interface through periodic heating.[128] (f) The voltage profiles of SSLSBs with varied active material loadings as a function of gravimetric capacity.[129] (g) Schematic of the proposed microstructure and discharge mechanism for the Li–S/VS_2 SSLSB.[129] (h) Schematic of the SSLSB based on PTTCA cathode (left) and detailed architectures of cathodes using PTTCA@SP and PTTCA@CNT composites (right).[130]

demonstrated a capacity of 629 mA h g^{-1} after 100 cycles with a small irreversible capacity loss in the first cycle (8.2%). In contrast, the liquid batteries showed rapid capacity decay and a significant irreversible capacity loss in the first cycle (44.6%). While for the case of iron disulfide (FeS_2) used as cathode additive materials, metallic Fe can form during discharge and disappear after charging. In non-aqueous electrolytes, FeS_2 can anchor and trap lithium polysulfides, aiding in the conversion from sulfur to Li_2S. However, in ether-based systems, using FeS_2 can cause capacity fading due to the dissolution of iron, which leads to the shuttling and deposition of iron sulfide in the anode region.[132,137]

Nazar group reported the development of an intercalation-conversion hybrid cathode that integrates intercalation-type VS_2 with conversion-type sulfur, resulting in a high-performance SSLSB.[129] Metallic VS_2 serves as the electronic conductor, delivering electrons. Additionally, lithiated vanadium sulfide (Li_xVS_2) can also conduct both ions and electrons. It has good Li-ion mobility between its atomic layers, allowing it to act as a Li-ion delivery vehicle during discharge and charge cycles as indicated in Fig. 6(f). Their work highlighted the impressive electrochemical performance of composite cathodes at high loading levels, with a stable areal capacity of up to 7.8 mA h cm^{-2} achieved at a high active material loading of 15.5 mg cm^{-2} as indicated in Fig. 6(g).

6.3 Sulfureous polymer materials

Sulfureous polymer materials consist of polymer units and sulfur chains, where sulfur atoms are covalently bonded to the organic framework. This structure ensures that sulfur is evenly dispersed, preventing clumping and enhancing sulfur utilization.[138] Additionally, the organic framework helps reduce the volume expansion that occurs during charging and discharging.[139] Sulfurized polyacrylonitrile (SPAN) was first introduced in 2002 as an alternative to sulfur for cathode materials and has since gained significant attention.[140] SPAN is a vulcanized polymer that leverages the interaction between the polymer's nitrile groups and elemental sulfur to destabilize polyacrylonitrile (PAN), promoting dehydrogenation and cyclization. The nitrile group's lone electron pair in PAN can easily interact with lithium through coordination bonds. Additionally, the SPAN cathode does not form long-chain polysulfides (PS) during discharge, allowing for

direct formation of Li_2S.[111] These properties result in high sulfur utilization, high coulombic efficiency, and cycling stability for the SPAN cathode. Sun group developed dense composite sulfur–carbon (S/C) cathodes using SPAN supported by a macroporous carbon (MaPC) conductive matrix, referred to as SPAN@MaPC, achieving a high reversible capacity of 1396.2 mA h g^{-1} at 0.1C and maintained a capacity of 715.5 mA h g^{-1} after 200 cycles.[141]

In addition to SPAN, a growing number of organic sulfur cathode materials have been developed and applied to SSLSBs. Gracai *et al.* used an inverse vulcanized sulfur copolymer as the cathode active material for poly(ethylene oxide) (PEO)-based Li–S cells to reduce the polysulfide shuttle effect and enhance the electrochemical performance of SSLSBs.[142] They synthesized the copolymer (p(S-DVB)) using a specific ratio of sulfur and 3,5-divinylbenzene, then mixed it with Ketjen black, a carbon material, and PEO electrolyte to create a composite cathode. The discharge/charge performance of the p(S-DVB) cathode was comparable to that of a traditional sulfur cathode. The SSLSB with the p(S-DVB) cathode delivered a capacity of 650 mA h g^{-1} at 0.1 C at 70 °C after 50 cycles. After 50 cycles, the membrane in the cell with the p(S-DVB) cathode remained clean without S-contained polymer as the active material in the cathode could reduce the polysulfide shuttle effect in PEO-based cells.

Yang *et al.* reported the organodisulfide cathode for SSLSBs by combining poly(trithiocyanuric acid) (PTTCA) with carbon nanotubes and $Li_7P_3S_{11}$ to improve the electronic and ionic conductivity of the cathode as illustrated in Fig. 6(h).[130] The Li–N coordination bond interaction between the PTTCA cathode and LPS electrolyte facilitated their intimate contact. PTTCA demonstrated much better interface compatibility with LPS compared to carbonyl-type poly(anthraquinonyl sulfide). This can be explained by the Hard and Soft Acids and Bases theory that predicts the most favorable interaction between metal ions and ligands and the potential catalytic effects they have on each other.[143] Consequently, the battery with PTTCA achieved a reversible capacity of 410 mA h g^{-1}, an energy density of 767 W h kg^{-1}, and a capacity retention of 83% after 100 cycles.

7. Outlook

SSLSBs offer compelling advantages over conventional LIBs, including high energy density, enhanced safety, cost-effectiveness, and environmental benignity compared to NMC-based ASSBs. To achieve high energy densities in SSLSBs, it is fundamental to follow the suggestions that we derived from the calculation.

1. Ensuring a sulfur loading of at least 4 mg cm^{-2} is crucial for attaining energy densities greater than 500 W h kg^{-1}.

2. Improving the utilization ratio of sulfur can significantly enhance energy density, which has the highest priority compared to increasing the sulfur content and lowering E/S.

3. The E/S ratio can lead to higher energy densities and should be lower than 5 to ensure an effective increase in the energy density.

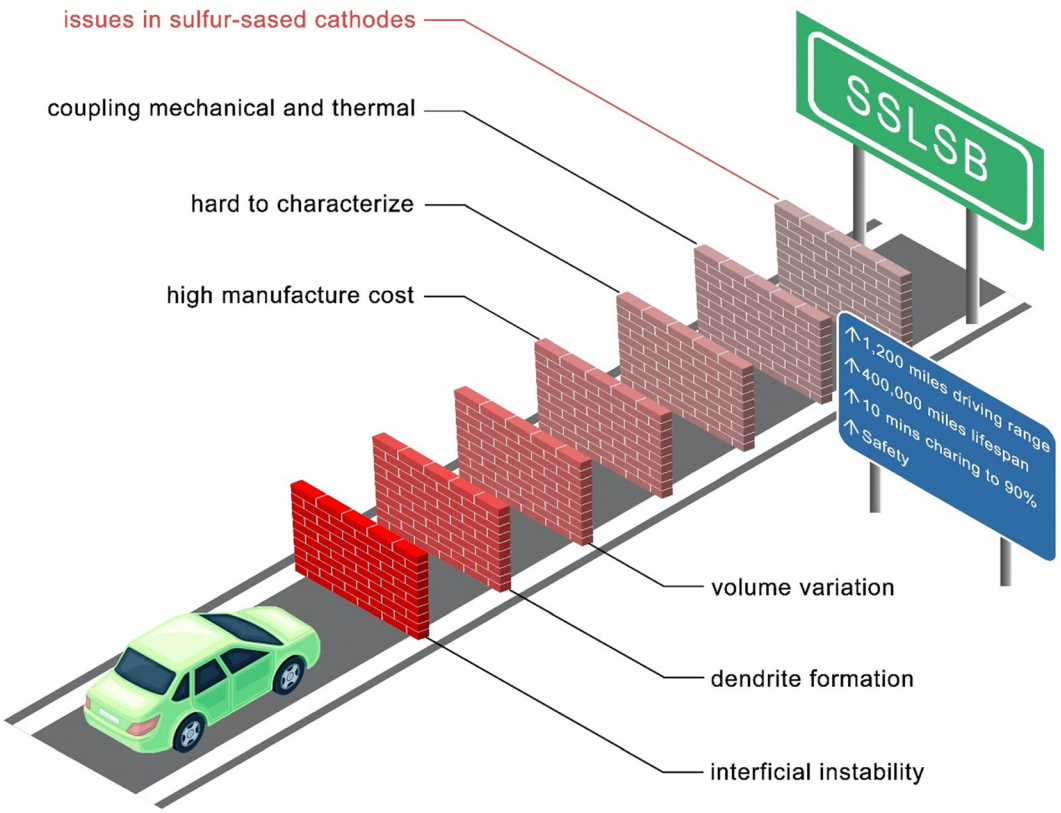

Fig. 7 The race towards the SSLSB.

4. Minimizing the negative-to-positive (N/P) ratio while ensuring the reversibility of lithium anodes is vital for enhancing energy density.

The practical implementation of these protocols involves intricate relationships between these variables. For instance, while increasing sulfur loading is essential, its benefits plateau beyond a certain point (around 4 mg cm^{-2}), making sulfur utilization improvements more impactful.

Despite these advantages, SSLSBs face several technical challenges that must be addressed to facilitate their commercial viability as illustrated in Fig. 7.

Common issues of all ASSBs such as interfacial instability, anode volume variation, and dendrite formation accelerating the degradation of the battery are major barriers. A reasonable cost for the manufacturing of SSLSBs is also essential to the practical application. Advancements in synthesis methods and scalability are crucial. More importantly, SSLSBs uniquely have sluggish ion transport within the bulk of sulfur and polysulfides. Additionally, limited by the characterization techniques and research focus, the understanding of the sulfur conversion process in various SSEs needs to be addressed. The rate-determined step in SSLSBs is also highly interesting to the sulfur cathode modification, which may help design the redox mediator for an effective catalysis path.

Several state-of-the-art modification strategies including developing sulfur–carbon composites and introducing metal sulfide additives have shown effectiveness in overcoming these challenges. In addition, utilizing sulfurized polymers such as sulfurized SPAN helps mitigate volume expansion and enhance sulfur utilization. However, while these strategies have shown promise, there remain several critical areas that require further exploration and innovation to fully realize the practical application of SSLSBs.

1. Developing advanced coating techniques is expected to improve the electrochemical and chemical stabilities at the interfaces of SSLSBs.

2. More attention should be given to using element doping and solid solutions to improve the electronic conductivity of sulfur and lithium sulfide rather than relying on carbon composites, as SSEs decompose when in contact with carbon materials.

3. Investigating cost-effective, scalable production methods for SSLSBs and their components is essential. Techniques new to the battery field, such as vapor deposition, hold valuable potential and should be explored.

4. Strategies for ensuring the integrity of cathode–electrolyte interfaces (CEIs) in ASSBs with NMC cathodes can offer valuable insights for the CEI design in SSLSBs.

By addressing these critical challenges and leveraging the outlined strategies, SSLSBs have the potential to significantly advance energy storage technologies, offering solutions that meet the high-energy demands and safety requirements of future applications.

Author contributions

Y. Z. contributed to Section 2, 3, and the Outlook of this review manuscript. F. Q. and J. B. contributed to Sections 5 and 6, respectively. D. L. and M. K. contributed to the Introduction and Section 4, H. S. arranged the funding and edited the manuscript, and S. L. conceptualized and supervised the manuscript, and arranged the funding.

Data availability

The data that support the findings of this study are available on request from the corresponding author.

Conflicts of interest

There are no conflicts to declare.

Acknowledgements

This work was supported by the US National Science Foundation, Award numbers CBET-2207302 and CMMI-2318677. SL and HWS acknowledge the support from the National Research Council of Science & Technology (NST) grant by the Korea Ministry of Science and ICT (MSIT) (CRC23021-000).

References

1 X.-G. Yang, T. Liu, S. Ge, E. Rountree and C.-Y. Wang, *Joule*, 2021, **5**, 1644–1659.
2 R. Goyal, C. Reiche, C. Fernando, J. Serrao, S. Kimmel, A. Cohen and S. Shaheen, Urban air mobility (UAM) market study, 2018.
3 A. Kasliwal, N. J. Furbush, J. H. Gawron, J. R. McBride, T. J. Wallington, R. D. De Kleine, H. C. Kim and G. A. Keoleian, *Nat. Commun.*, 2019, **10**, 1555.
4 B. R. Sutherland, *Joule*, 2019, **3**, 1187–1189.
5 J. Holden and N. Goel, *Fast-forwarding to a future of on-demand urban air transportation*, San Francisco, CA, 2016.
6 P. Albertus, V. Anandan, C. Ban, N. Balsara, I. Belharouak, J. Buettner-Garrett, Z. Chen, C. Daniel, M. Doeff, N. J. Dudney, B. Dunn, S. J. Harris, S. Herle, E. Herbert, S. Kalnaus, J. A. Libera, D. Lu, S. Martin, B. D. McCloskey, M. T. McDowell, Y. S. Meng, J. Nanda, J. Sakamoto, E. C. Self, S. Tepavcevic, E. Wachsman, C. Wang, A. S. Westover, J. Xiao and T. Yersak, *ACS Energy Lett.*, 2021, **6**, 1399–1404.
7 J. W. Choi and D. Aurbach, *Nat. Rev. Mater.*, 2016, **1**, 1–16.
8 P. G. Bruce, S. A. Freunberger, L. J. Hardwick and J.-M. Tarascon, *Nat. Mater.*, 2012, **11**, 19–29.
9 Z. P. Cano, D. Banham, S. Ye, A. Hintennach, J. Lu, M. Fowler and Z. Chen, *Nat. Energy*, 2018, **3**, 279–289.
10 Q. Pang, X. Liang, C. Y. Kwok and L. F. Nazar, *Nat. Energy*, 2016, **1**, 1–11.
11 A. Manthiram, Y. Fu and Y.-S. Su, *Acc. Chem. Res.*, 2013, **46**, 1125–1134.
12 Z. W. Seh, Y. Sun, Q. Zhang and Y. Cui, *Chem. Soc. Rev.*, 2016, **45**, 5605–5634.
13 Y. Chen, T. Wang, H. Tian, D. Su, Q. Zhang and G. Wang, *Adv. Mater.*, 2021, **33**, 2003666.

14 S. Sripad and V. Viswanathan, *Proc. Natl. Acad. Sci. U. S. A.*, 2021, **118**, e2111164118.
15 W. L. Fredericks, S. Sripad, G. C. Bower and V. Viswanathan, *ACS Energy Lett.*, 2018, **3**, 2989–2994.
16 A. Bills, S. Sripad, W. L. Fredericks, M. Singh and V. Viswanathan, *ACS Energy Lett.*, 2020, **5**, 663–668.
17 M. Warren, A. Garbo, M. T. K. Herniczek, T. Hamilton and B. German, AIAA Scitech 2019 Forum, DOI: 10.2514/6.2019-0527.
18 T. Liu, X.-G. Yang, S. Ge, Y. Leng and C.-Y. Wang, *ETransportation*, 2021, **7**, 100103.
19 Y. Zhang, J. C. Kim, H. W. Song and S. Lee, *Nanoscale*, 2023, **15**, 4195–4218.
20 Y. Liu, Y. Zhu and Y. Cui, *Nat. Energy*, 2019, **4**, 540–550.
21 S. Zhang, K. Xu and T. Jow, *J. Power Sources*, 2003, **115**, 137–140.
22 N. Zhang, T. Deng, S. Zhang, C. Wang, L. Chen, C. Wang and X. Fan, *Adv. Mater.*, 2022, **34**, 2107899.
23 D. Hubble, D. E. Brown, Y. Zhao, C. Fang, J. Lau, B. D. McCloskey and G. Liu, *Energy Environ. Sci.*, 2022, **15**, 550–578.
24 D. H. Tan, Y. S. Meng and J. Jang, *Joule*, 2022, **6**, 1755–1769.
25 U.-H. Kim, T.-Y. Yu, J. W. Lee, H. U. Lee, I. Belharouak, C. S. Yoon and Y.-K. Sun, *ACS Energy Lett.*, 2023, **8**, 809–817.
26 Y.-K. Sun, *ACS Energy Lett.*, 2020, **5**, 3221–3223.
27 A. M. Bates, Y. Preger, L. Torres-Castro, K. L. Harrison, S. J. Harris and J. Hewson, *Joule*, 2022, **6**, 742–755.
28 J. Schnell, H. Knörzer, A. J. Imbsweiler and G. Reinhart, *Energy Technol.*, 2020, **8**, 1901237.
29 D. Karabelli, K. P. Birke and M. Weeber, *Batteries*, 2021, **7**, 18.
30 C. Singer, J. Schnell and G. Reinhart, *Energy Technol.*, 2021, **9**, 2000665.
31 N. Jones, *Nature*, 2024, **626**, 248–251.
32 K. Liu, Y. Liu, D. Lin, A. Pei and Y. Cui, *Sci. Adv.*, 2018, **4**, eaas9820.
33 Y. Chen, Y. Kang, Y. Zhao, L. Wang, J. Liu, Y. Li, Z. Liang, X. He, X. Li and N. Tavajohi, *J. Energy Chem.*, 2021, **59**, 83–99.
34 D. H. Doughty and E. P. Roth, *Electrochem. Soc. Interface*, 2012, **21**, 37.
35 J. Charbonnel, N. Darmet, C. Deilhes, L. Broche, M. Reytier, P.-X. Thivel and R. Vincent, *ACS Appl. Energy Mater.*, 2022, **5**, 10862–10871.
36 C. Wang, J. T. Kim, C. Wang and X. Sun, *Adv. Mater.*, 2023, **35**, 2209074.
37 R. Chen, Q. Li, X. Yu, L. Chen and H. Li, *Chem. Rev.*, 2020, **120**, 6820–6877.
38 C.-Y. Wang, T. Liu, X.-G. Yang, S. Ge, N. V. Stanley, E. S. Rountree, Y. Leng and B. D. McCarthy, *Nature*, 2022, **611**, 485–490.
39 R. S. Longchamps, X.-G. Yang and C.-Y. Wang, *ACS Energy Lett.*, 2022, **7**, 1103–1111.
40 S. Xu, Z. Sun, C. Sun, F. Li, K. Chen, Z. Zhang, G. Hou, H. M. Cheng and F. Li, *Adv. Funct. Mater.*, 2020, **30**, 2007172.
41 J. Hou, M. Yang, D. Wang and J. Zhang, *Adv. Energy Mater.*, 2020, **10**, 1904152.
42 H. Song, S. Wang, X. Song, J. Wang, K. Jiang, S. Huang, M. Han, J. Xu, P. He, K. Chen and H. Zhou, *Energy Environ. Sci.*, 2020, **13**, 1205–1211.
43 NASA, Solid-State Lithium–Sulfur Battery Tech Portfolio, https://technology.nasa.gov/patent/LEW-TOPS-167.
44 Q. Zhao, S. Stalin, C.-Z. Zhao and L. A. Archer, *Nat. Rev. Mater.*, 2020, **5**, 229–252.
45 Y. Xiao, Y. Wang, S.-H. Bo, J. C. Kim, L. J. Miara and G. Ceder, *Nat. Rev. Mater.*, 2020, **5**, 105–126.
46 Y. Zheng, Y. Yao, J. Ou, M. Li, D. Luo, H. Dou, Z. Li, K. Amine, A. Yu and Z. Chen, *Chem. Soc. Rev.*, 2020, **49**, 8790–8839.
47 B. L. Ellis, K. T. Lee and L. F. Nazar, *Chem. Mater.*, 2010, **22**, 691–714.
48 A. Manthiram, *Nat. Commun.*, 2020, **11**, 1550.
49 A. Banerjee, X. Wang, C. Fang, E. A. Wu and Y. S. Meng, *Chem. Rev.*, 2020, **120**, 6878–6933.
50 D. Larcher and J. M. Tarascon, *Nat. Chem.*, 2015, **7**, 19–29.
51 P. A. Nelson, S. Ahmed, K. G. Gallagher and D. W. Dees, *Modeling the Performance and Cost of Lithium-Ion Batteries for Electric-Drive Vehicles*, 3rd edn, USA, 2019.
52 P. A. Nelson, K. G. Gallagher, I. D. Bloom and D. W. Dees, *Modeling the Performance and Cost of Lithium-Ion Batteries for Electric-Drive Vehicles*, 2nd edn, USA, 2012.
53 L. Gaines and R. Cuenca, *Costs of lithium-ion batteries for vehicles*, USA, 2000.
54 S. Mallick, A. Patel, X.-G. Sun, M. P. Paranthaman, M. Mou, J. H. Mugumya, M. Jiang, M. L. Rasche, H. Lopez and R. B. Gupta, *J. Mater. Chem. A*, 2023, **11**, 3789–3821.
55 N. T. Nassar, T. E. Graedel and E. M. Harper, *Sci. Adv.*, 2015, **1**, e1400180.
56 C. Vaalma, D. Buchholz, M. Weil and S. Passerini, *Nat. Rev. Mater.*, 2018, **3**, 18013.
57 A. E. Saal, E. H. Hauri, C. H. Langmuir and M. R. Perfit, *Nature*, 2002, **419**, 451–455.
58 T. C. Institute, Application of cobalt in rechargeable batteries, https://www.cobaltinstitute.org/rechargeable-batteries.html, 2018.
59 Y. Zhang, C. S. Kim, H. W. Song, S.-J. Chang, H. Kim, J. Park, S. Hu, K. Zhao and S. Lee, *Energy Storage Mater.*, 2022, **48**, 1–11.
60 G. Pistoia, *Lithium-Ion Batteries: Advances and Applications*, Newnes, 2013.
61 A. International, This is what we die for.' Human rights abuses in the Democratic Republic of the Congo power the global trade in cobalt, https://www.amnestyusa.org/files/this_what_we_die_for_-_report.pdf.
62 S.-T. Myung, F. Maglia, K.-J. Park, C. S. Yoon, P. Lamp, S.-J. Kim and Y.-K. Sun, *ACS Energy Lett.*, 2017, **2**, 196–223.
63 M. M. Thackeray, S.-H. Kang, C. S. Johnson, J. T. Vaughey, R. Benedek and S. A. Hackney, *J. Mater. Chem.*, 2007, **17**, 3112–3125.
64 T. Economics, https://tradingeconomics.com/commodity/nickel.

65 J. Leszczynski, *Handbook of Computational Chemistry*, Springer, Netherlands, 2012.
66 G. Zhou, H. Chen and Y. Cui, *Nat. Energy*, 2022, **7**, 312–319.
67 C. Wang, J. T. Kim, C. Wang and X. Sun, *Adv. Mater.*, 2023, **35**, 2209074.
68 S. Zhang, J. Ma, S. Dong and G. Cui, *Electrochem. Energy Rev.*, 2023, **6**, 4.
69 B. Qi, X. Hong, Y. Jiang, J. Shi, M. Zhang, W. Yan and C. Lai, *Nano-Micro Lett.*, 2024, **16**, 71.
70 X. Yu and A. Manthiram, *Acc. Chem. Res.*, 2017, **50**, 2653–2660.
71 S. Li, S.-J. Yang, G.-X. Liu, J.-K. Hu, Y.-L. Liao, X.-L. Wang, R. Wen, H. Yuan, J.-Q. Huang and Q. Zhang, *Adv. Mater.*, 2024, **36**, 2307768.
72 H. Lim, S. Jun, Y. B. Song, H. Bae, J. H. Kim and Y. S. Jung, *Energy Storage Mater.*, 2022, **50**, 543–553.
73 Y. Morino, H. Sano, K. Kawamoto, K.-I. Fukui, M. Takeuchi, A. Sakuda and A. Hayashi, *Solid State Ionics*, 2023, **392**, 116162.
74 H. Kiuchi, K. Hikima, K. Shimizu, R. Kanno, F. Toshiharu and E. Matsubara, *Electrochem. Commun.*, 2020, **118**, 106790.
75 C. Chen, M. Jiang, T. Zhou, L. Raijmakers, E. Vezhlev, B. Wu, T. U. Schülli, D. L. Danilov, Y. Wei, R.-A. Eichel and P. H. L. Notten, *Adv. Energy Mater.*, 2021, **11**, 2003939.
76 C. Yuan, X. Gao, Y. Jia, W. Zhang, Q. Wu and J. Xu, *Nano Energy*, 2021, **86**, 106057.
77 C. Yuan, W. Lu and J. Xu, *Adv. Energy Mater.*, 2021, **11**, 2101807.
78 S. Wenzel, S. Randau, T. Leichtweiß, D. A. Weber, J. Sann, W. G. Zeier and J. Janek, *Chem. Mater.*, 2016, **28**, 2400–2407.
79 F. Han, Y. Zhu, X. He, Y. Mo and C. Wang, *Adv. Energy Mater.*, 2016, **6**, 1501590.
80 G. Bucci, B. Talamini, A. Renuka Balakrishna, Y.-M. Chiang and W. C. Carter, *Phys. Rev. Mater.*, 2018, **2**, 105407.
81 H. Fathiannasab, L. Zhu and Z. Chen, *J. Power Sources*, 2021, **483**, 229028.
82 G. Deysher, P. Ridley, S.-Y. Ham, J.-M. Doux, Y.-T. Chen, E. A. Wu, D. H. S. Tan, A. Cronk, J. Jang and Y. S. Meng, *Mater. Today Phys.*, 2022, **24**, 100679.
83 J.-M. Doux, H. Nguyen, D. H. S. Tan, A. Banerjee, X. Wang, E. A. Wu, C. Jo, H. Yang and Y. S. Meng, *Adv. Energy Mater.*, 2020, **10**, 1903253.
84 R. Guo, K. Zhang, W. Zhao, Z. Hu, S. Li, Y. Zhong, R. Yang, X. Wang, J. Wang, C. Wu and Y. Bai, *Energy Mater. Adv.*, 2023, **4**, 0022.
85 Y. Chen, W. Li, C. Sun, J. Jin, Q. Wang, X. Chen, W. Zha and Z. Wen, *Adv. Energy Mater.*, 2021, **11**, 2002545.
86 S. Wang, Y. Wu, H. Li, L. Chen and F. Wu, *InfoMat*, 2022, **4**, e12316.
87 S. Wang, Y. Wu, T. Ma, L. Chen, H. Li and F. Wu, *ACS Nano*, 2022, **16**, 16158–16176.
88 Y. Nikodimos, C.-J. Huang, B. W. Taklu, W.-N. Su and B. J. Hwang, *Energy Environ. Sci.*, 2022, **15**, 991–1033.
89 R. Chen, A. M. Nolan, J. Lu, J. Wang, X. Yu, Y. Mo, L. Chen, X. Huang and H. Li, *Joule*, 2020, **4**, 812–821.
90 L. Xu, J. Li, W. Deng, H. Shuai, S. Li, Z. Xu, J. Li, H. Hou, H. Peng, G. Zou and X. Ji, *Adv. Energy Mater.*, 2021, **11**, 2000648.
91 L. Cheng, M. Liu, A. Mehta, H. Xin, F. Lin, K. Persson, G. Chen, E. J. Crumlin and M. Doeff, *ACS Appl. Energy Mater.*, 2018, **1**, 7244–7252.
92 N. Zhang, G. Ren, L. Li, Z. Wang, P. Yu, X. Li, J. Zhou, H. Zhang, L. Zhang, Z. Liu and X. Liu, *Nat. Commun.*, 2024, **15**, 2777.
93 J. Schnell, F. Tietz, C. Singer, A. Hofer, N. Billot and G. Reinhart, *Energy Environ. Sci.*, 2019, **12**, 1818–1833.
94 D. H. S. Tan, A. Banerjee, Z. Chen and Y. S. Meng, *Nat. Nanotechnol.*, 2020, **15**, 170–180.
95 H.-D. Lim, J.-H. Park, H.-J. Shin, J. Jeong, J. T. Kim, K.-W. Nam, H.-G. Jung and K. Y. Chung, *Energy Storage Mater.*, 2020, **25**, 224–250.
96 H. Xu, Y. Yu, Z. Wang and G. Shao, *Energy Environ. Mater.*, 2019, **2**, 234–250.
97 M. Alabdali, F. M. Zanotto, V. Viallet, V. Seznec and A. A. Franco, *Curr. Opin. Electrochem.*, 2022, **36**, 101127.
98 Z. Zheng, J. Zhou and Y. Zhu, *Chem. Soc. Rev.*, 2024, **53**, 3134–3166.
99 T. Lombardo, M. Duquesnoy, H. El-Bouysidy, F. Årén, A. Gallo-Bueno, P. B. Jørgensen, A. Bhowmik, A. Demortière, E. Ayerbe, F. Alcaide, M. Reynaud, J. Carrasco, A. Grimaud, C. Zhang, T. Vegge, P. Johansson and A. A. Franco, *Chem. Rev.*, 2022, **122**, 10899–10969.
100 Y. Zhang, H. W. Song, K. R. Crompton, X. Yang, K. Zhao and S. Lee, *Nano Energy*, 2023, **115**, 108756.
101 Y. Lin, J. Zheng, C. Wang and Y. Qi, *Nano Energy*, 2020, **75**, 104915.
102 S. Rehman, M. Pope, S. Tao and E. McCalla, *Energy Environ. Sci.*, 2022, **15**, 1423–1460.
103 J. Gu, Z. Liang, J. Shi and Y. Yang, *Adv. Energy Mater.*, 2023, **13**, 2203153.
104 X. Yang, J. Luo and X. Sun, *Chem. Soc. Rev.*, 2020, **49**, 2140–2195.
105 D. Cao, X. Sun, F. Li, S.-M. Bak, T. Ji, M. Geiwitz, K. S. Burch, Y. Du, G. Yang and H. Zhu, *Angew. Chem., Int. Ed.*, 2023, **62**, e202302363.
106 R. Bradbury, G. F. Dewald, M. A. Kraft, T. Arlt, N. Kardjilov, J. Janek, I. Manke, W. G. Zeier and S. Ohno, *Adv. Energy Mater.*, 2023, **13**, 2203426.
107 T. Liu, H. Hu, X. Ding, H. Yuan, C. Jin, J. Nai, Y. Liu, Y. Wang, Y. Wan and X. Tao, *Energy Storage Mater.*, 2020, **30**, 346–366.
108 Y. Yang, G. Zheng and Y. Cui, *Chem. Soc. Rev.*, 2013, **42**, 3018–3032.
109 M. Weiss, R. Ruess, J. Kasnatscheew, Y. Levartovsky, N. R. Levy, P. Minnmann, L. Stolz, T. Waldmann, M. Wohlfahrt-Mehrens, D. Aurbach, M. Winter, Y. Ein-Eli and J. Janek, *Adv. Energy Mater.*, 2021, **11**, 2101126.
110 B. Ding, J. Wang, Z. Fan, S. Chen, Q. Lin, X. Lu, H. Dou, A. Kumar Nanjundan, G. Yushin, X. Zhang and Y. Yamauchi, *Mater. Today*, 2020, **40**, 114–131.

111 R. Kumar, J. Liu, J.-Y. Hwang and Y.-K. Sun, *J. Mater. Chem. A*, 2018, **6**, 11582–11605.
112 Y. Wang, E. Sahadeo, G. Rubloff, C.-F. Lin and S. B. Lee, *J. Mater. Sci.*, 2019, **54**, 3671–3693.
113 C. Xing, H. Chen, S. Qian, Z. Wu, A. Nizami, X. Li, S. Zhang and C. Lai, *Chem*, 2022, **8**, 1201–1230.
114 X. Zhu, L. Wang, Z. Bai, J. Lu and T. Wu, *Nano-Micro Lett.*, 2023, **15**, 75.
115 M. Yu, Z. Wang, Y. Wang, Y. Dong and J. Qiu, *Adv. Energy Mater.*, 2017, **7**, 1700018.
116 J. Jiang, Q. Fan, S. Chou, Z. Guo, K. Konstantinov, H. Liu and J. Wang, *Small*, 2021, **17**, 1903934.
117 S. Luo, F. Wu and G. Yushin, *Mater. Today*, 2021, **49**, 253–270.
118 H. Ye, M. Li, T. Liu, Y. Li and J. Lu, *ACS Energy Lett.*, 2020, **5**, 2234–2245.
119 S. Li, D. Leng, W. Li, L. Qie, Z. Dong, Z. Cheng and Z. Fan, *Energy Storage Mater.*, 2020, **27**, 279–296.
120 X. Yao, N. Huang, F. Han, Q. Zhang, H. Wan, J. P. Mwizerwa, C. Wang and X. Xu, *Adv. Energy Mater.*, 2017, **7**, 1602923.
121 H. Yan, H. Wang, D. Wang, X. Li, Z. Gong and Y. Yang, *Nano Lett.*, 2019, **19**, 3280–3287.
122 A. S. Alzahrani, M. Otaki, D. Wang, Y. Gao, T. S. Arthur, S. Liu and D. Wang, *ACS Energy Lett.*, 2021, **6**, 413–418.
123 Y. Luo, R. Guo, T. Li, F. Li, Z. Liu, M. Zheng, B. Wang, Z. Yang, H. Luo and Y. Wan, *ChemSusChem*, 2019, **12**, 1591–1611.
124 X. Hong, Y. Liu, Y. Li, X. Wang, J. Fu and X. Wang, *Polymers*, 2020, **12**, 331.
125 P. T. Dirlam, R. S. Glass, K. Char and J. Pyun, *J. Polym. Sci., Part A: Polym. Chem.*, 2017, **55**, 1635–1668.
126 G.-L. Xu, J. Liu, R. Amine, Z. Chen and K. Amine, *ACS Energy Lett.*, 2017, **2**, 605–614.
127 X. Li, J. Liang, J. Luo, C. Wang, X. Li, Q. Sun, R. Li, L. Zhang, R. Yang, S. Lu, H. Huang and X. Sun, *Adv. Mater.*, 2019, **31**, 1808100.
128 J. Zhou, M. L. Holekevi Chandrappa, S. Tan, S. Wang, C. Wu, H. Nguyen, C. Wang, H. Liu, S. Yu, Q. R. S. Miller, G. Hyun, J. Holoubek, J. Hong, Y. Xiao, C. Soulen, Z. Fan, E. E. Fullerton, C. J. Brooks, C. Wang, R. J. Clément, Y. Yao, E. Hu, S. P. Ong and P. Liu, *Nature*, 2024, **627**, 301–305.
129 S. Kim, J. Choi, S.-M. Bak, L. Sang, Q. Li, A. Patra and P. V. Braun, *Adv. Funct. Mater.*, 2019, **29**, 1901719.
130 Z. Yang, F. Wang, Z. Hu, J. Chu, H. Zhan, X. Ai and Z. Song, *Adv. Energy Mater.*, 2021, **11**, 2102962.
131 N. H. H. Phuc, M. Takaki, M. Hiroyuki and M. Atsunori, *Front. Energy Res.*, 2021, **8**, 606023.
132 J. P. Mwizerwa, Q. Zhang, F. Han, H. Wan, L. Cai, C. Wang and X. Yao, *ACS Appl. Mater. Interfaces*, 2020, **12**, 18519–18525.
133 M. Chen, R. Prasada Rao and S. Adams, *Solid State Ionics*, 2014, **268**, 300–304.
134 S. Xu, C. Y. Kwok, L. Zhou, Z. Zhang, I. Kochetkov and L. F. Nazar, *Adv. Funct. Mater.*, 2021, **31**, 2004239.
135 A. Hayashi, T. Ohtomo, F. Mizuno, K. Tadanaga and M. Tatsumisago, *Electrochim. Acta*, 2004, **50**, 893–897.
136 J. Gu, H. Zhong, Z. Chen, J. Shi, Z. Gong and Y. Yang, *Chem. Eng. J.*, 2023, **454**, 139923.
137 U. Ulissi, S. Ito, S. M. Hosseini, A. Varzi, Y. Aihara and S. Passerini, *Adv. Energy Mater.*, 2018, **8**, 1801462.
138 W. Zhang, Y. Zhang, L. Peng, S. Li, X. Wang, S. Cheng and J. Xie, *Nano Energy*, 2020, **76**, 105083.
139 X. Zhang, K. Chen, Z. Sun, G. Hu, R. Xiao, H.-M. Cheng and F. Li, *Energy Environ. Sci.*, 2020, **13**, 1076–1095.
140 J. Wang, J. Yang, J. Xie and N. Xu, *Adv. Mater.*, 2002, **14**, 963–965.
141 Z. Sun, Y. Hu, F. Qin, N. Lv, B. Li, L. Jiang, Z. Zhang and F. Liu, *Sustainable Energy Fuels*, 2021, **5**, 5603–5614.
142 I. Gracia, H. Ben Youcef, X. Judez, U. Oteo, H. Zhang, C. Li, L. M. Rodriguez-Martinez and M. Armand, *J. Power Sources*, 2018, **390**, 148–152.
143 G. Sahu, Z. Lin, J. Li, Z. Liu, N. Dudney and C. Liang, *Energy Environ. Sci.*, 2014, **7**, 1053–1058.